Acta Crystallographica Section D
Biological Crystallography
ISSN 1399-0047

Identification of a novel polyfluorinated compound as a lead to inhibit the human enzymes aldose reductase and AKR1B10: structure determination of both ternary complexes and implications for drug design

Alexandra Cousido-Siah,[a]‡ Francesc X. Ruiz,[a,b]‡ André Mitschler,[a] Sergio Porté,[b] Ángel R. de Lera,[c] María J. Martín,[d] Sonia Manzanaro,[d] Jesús A. de la Fuente,[d] Felix Terwesten,[e] Michael Betz,[e] Gerhard Klebe,[e] Jaume Farrés,[b] Xavier Parés[b] and Alberto Podjarny[a]*

[a]Department of Integrative Biology, Institut de Génétique et de Biologie Moléculaire et Cellulaire, CNRS/INSER/UdS, 1 Rue Laurent Fries, 67404 Illkirch CEDEX, France, [b]Department of Biochemistry and Molecular Biology, Universitat Autònoma de Barcelona, Bellaterra, 08193 Barcelona, Spain, [c]Departamento de Química Orgánica, Universidade de Vigo, 36310 Vigo, Spain, [d]Biomar Microbial Technologies S.A., Parque Tecnológico de León, 24009 León, Spain, and [e]Department of Pharmaceutical Chemistry, University of Marburg, Marbacher Weg 6, 35032 Marburg, Germany

‡ These authors contributed equally to this work.

Correspondence e-mail: podjarny@igbmc.fr

Received 23 May 2013
Accepted 10 December 2013

PDB references: AR–NADP$^+$–JF0064 complex, 4igs; AKR1B10–NADP$^+$–JF0064 complex, 4icc

Aldo-keto reductases (AKRs) are mostly monomeric enzymes which fold into a highly conserved $(\alpha/\beta)_8$ barrel, while their substrate specificity and inhibitor selectivity are determined by interaction with residues located in three highly variable external loops. The closely related human enzymes aldose reductase (AR or AKR1B1) and AKR1B10 are of biomedical interest because of their involvement in secondary diabetic complications (AR) and in cancer, *e.g.* hepatocellular carcinoma and smoking-related lung cancer (AKR1B10). After characterization of the IC_{50} values of both AKRs with a series of polyhalogenated compounds, 2,2′,3,3′,5,5′,6,6′-octafluoro-4,4′-biphenyldiol (JF0064) was identified as a lead inhibitor of both enzymes with a new scaffold (a 1,1′-biphenyl-4,4′-diol). An ultrahigh-resolution X-ray structure of the AR–NADP$^+$–JF0064 complex has been determined at 0.85 Å resolution, allowing it to be observed that JF0064 interacts with the catalytic residue Tyr48 through a negatively charged hydroxyl group (*i.e.* the acidic phenol). The non-competitive inhibition pattern observed for JF0064 with both enzymes suggests that this acidic hydroxyl group is also present in the case of AKR1B10. Moreover, the combination of surface lysine methylation and the introduction of K125R and V301L mutations enabled the determination of the X-ray crystallographic structure of the corresponding AKR1B10–NADP$^+$–JF0064 complex. Comparison of the two structures has unveiled some important hints for subsequent structure-based drug-design efforts.

1. Introduction

Human aldose reductase (AR; also known as AKR1B1) enzymatically transforms excessive cytosolic glucose into sorbitol through hydride donation from its cofactor NADPH (which becomes NADP$^+$) and proton donation from the enzyme. Sorbitol is a molecule which poorly penetrates cell membranes and is sometimes slowly metabolized. Therefore, hyperglycaemia may cause intracellular accumulation of sorbitol and its metabolite fructose, which may produce osmotic swelling and cell dysfunction. This simple paradigm configured the ‘Osmotic Hypothesis’ for diabetic complications and was armed with positive pre-clinical results on prototype AR inhibitors (ARIs), as researchers worldwide have targeted secondary diabetic complications with ARIs for

four decades. However, most trial outcomes have been disappointing, even as scientific evidence that AR plays a key pathogenic role in diabetes has continued to mount. In cells cultured under high-glucose conditions, many studies have demonstrated similarly AR-dependent increases in oxidative stress, confirming AR as an important factor in the pathogenesis of many diabetic complications. Also, ARIs may be able to prevent or delay the onset of cardiovascular complications such as ischaemia/reperfusion injury, atherosclerosis and atherothrombosis related to secondary diabetic complications (Tang *et al.*, 2012). Evidence is now strong that the Osmotic Hypothesis and the nerve sorbitol endpoint were misleading. Current recognition of the pathogenic importance of oxidative stress and its strong link to metabolic flux through AR have led to a revitalized 'Metabolic Flux Hypothesis' emphasizing cofactor rather than polyol turnover (Oates, 2008). Moreover, AR has recently been related to a number of inflammatory diseases such as atherosclerosis, sepsis, asthma, allergic rhinitis and uveitis (Ramana & Srivastava, 2010; Yadav *et al.*, 2013). Furthermore, AR has been shown to be involved in cancer, especially colon and hepatocellular carcinomas (Tammali *et al.*, 2011; Zeindl-Eberhart *et al.*, 2004), and AR inhibition has been reported to prevent colon cancer metastasis (Tammali *et al.*, 2011).

AKR1B10 is an AR homologue (sharing 71% sequence identity) that is primarily found in the colon, small intestine and adrenal glands, and is overexpressed in lung and liver cancers, amongst others (Fukumoto *et al.*, 2005; Ruiz *et al.*, 2009; Wang *et al.*, 2009; Zeindl-Eberhart *et al.*, 2004). This enzyme is able to catalyze the reduction of anticancer and potentially cytostatic drugs, and of different kinds of aldehydes, but does not catalyze the reduction of glucose (Barski *et al.*, 2008; Gallego *et al.*, 2006). AKR1B10 can reduce retinaldehyde to retinol, thus depleting intracellular retinoic acid (RA). AKR1B10 may impact on the carcinogenesis process through different pathways, *e.g.* the control of RA signalling (Gallego *et al.*, 2007; Penning, 2005; Quinn *et al.*, 2008; Ruiz *et al.*, 2009, 2012), detoxification of reactive lipid aldehydes, promotion of lipid synthesis by association with acetyl-CoA carboxylase and regulation of protein isoprenylation (Chung *et al.*, 2012; Ma *et al.*, 2008; Wang *et al.*, 2010). It is especially noteworthy that tobacco smoking mediates AKR1B10 overexpression in the airway epithelia of smokers with no previous evidence of lung cancer. In the context of

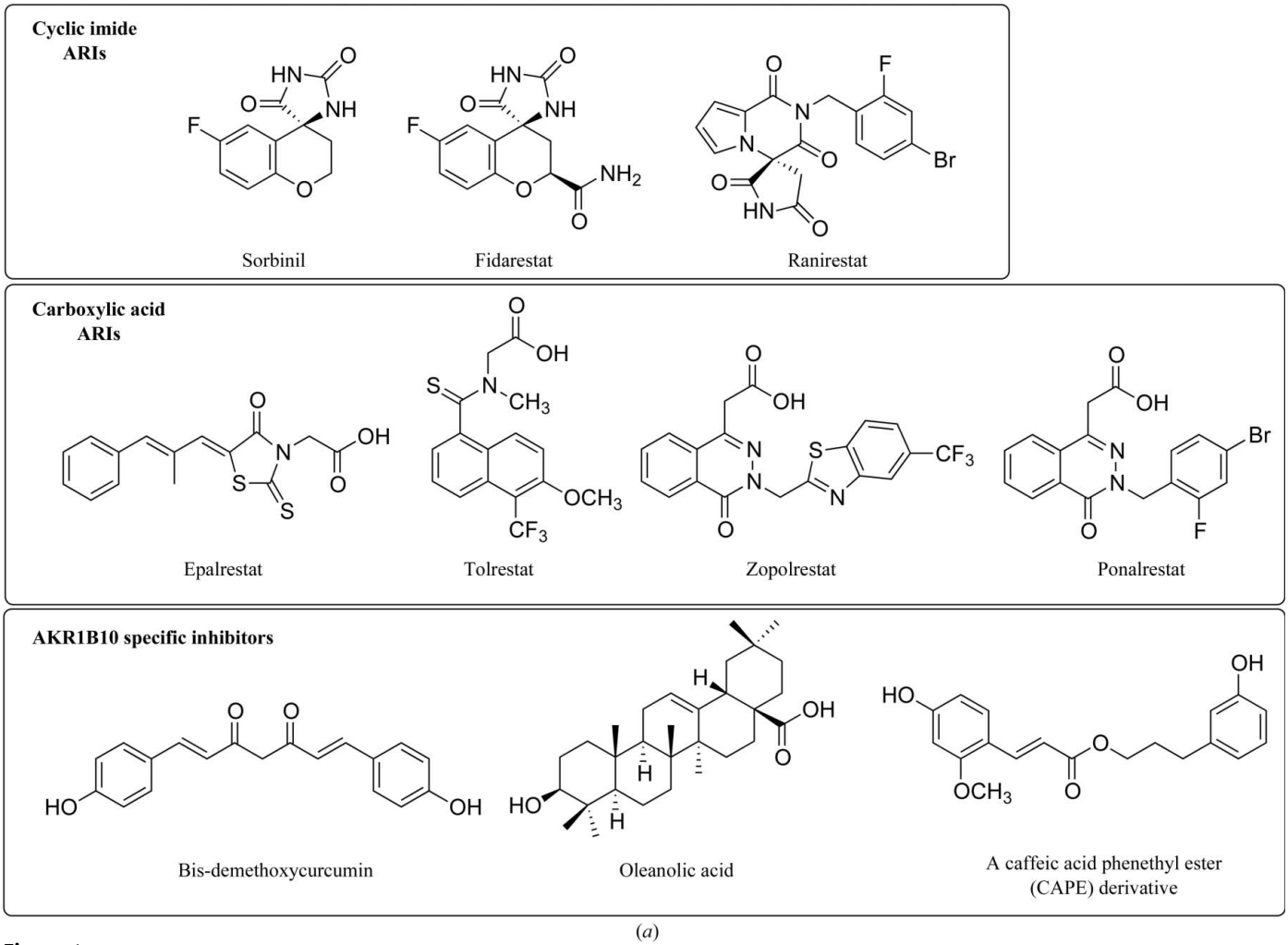

(*a*)

Figure 1
(*a*) Chemical structures of some representative ARIs and AKR1B10 inhibitors.

these observations and the link of AKR1B10 with the metabolism of retinoids and with lung cancer, the smoking-induced up-regulation of AKR1B10 may be an early process in the multiple events leading to lung cancer (Wang *et al.*, 2010). AKR1B10 also catalyzes the reduction of anticancer drugs such as daunorubicin, oracin and idarubicin, which is also thought to cause cancer cell chemoresistance. Thus, this enzyme has been recognized not only as a potential diagnostic and/or prognostic marker, but also as a target for the prevention and treatment of different types of cancer (Soda, Hu *et al.*, 2012).

Most ARIs contain a carboxylic acid moiety or a cyclic imide group (Fig. 1*a*). The best known of the cyclic imide compounds, sorbinil, has been thoroughly analyzed by structure determination of its ternary complex with AR and $NADP^+$ and also by several clinical studies. Other examples of this group of compounds include fidarestat and ranirestat. There are also numerous compounds that incorporate a carboxylic acid moiety, such as tolrestat, ponalrestat and zopolrestat. The cyclic imide or carboxylic acid moiety binds to an essentially hydrophilic area of the active site of AR, the anion-binding pocket, which involves the catalytic residues Tyr48 and His110, along with Trp111 and the positively charged nicotinamide moiety of the cofactor $NADP^+$. Another feature common to the various inhibitors is the presence of one or more aromatic groups, which bind in a hydrophobic pocket of AR bordered by the Trp111, Phe122 and Leu300 residues through hydrogen bonding and hydrophobic contacts. This constitutes a second important pharmacophoric requirement for inhibitors binding to AR. In most cases, this second pocket, known as the 'specificity pocket', is open and is well differentiated from the anion-binding pocket. All of these features of the ARIs have been extensively reviewed (Changjin, 2013; El-Kabbani & Podjarny, 2007; Oates, 2008).

Inhibitors containing the carboxylic acid or cyclic imide group exhibit similar *in vitro* activities but different *in vivo*

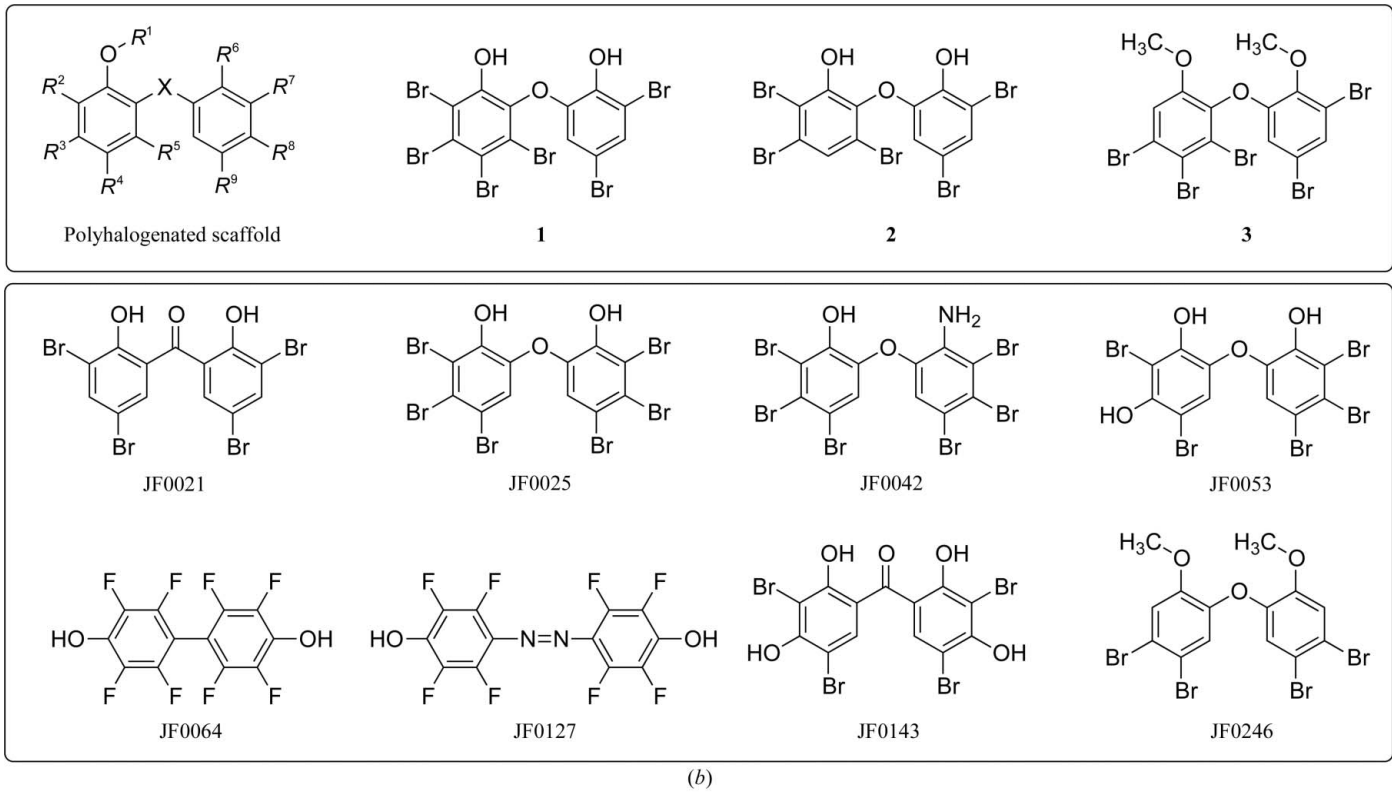

(*b*)

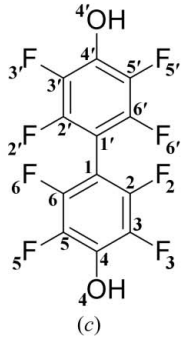

(*c*)

Figure 1 (continued)
(*b*) Chemical structures of the parent synthesis scaffold, marine sponge natural products and the JF inhibitor series. (*c*) The JF0064 chemical structure with the numbering used in both PDB entries. Chemical structures were prepared with *ChemDraw*.

activities. The carboxylic acid-containing inhibitors have lower *in vivo* activity, which has been attributed to the relatively low pK_a value of the carboxyl group, thus causing ionization at physiological pH and an inability to traverse cell membranes. Conversely, cyclic imides have higher pK_a values and are only partially ionized at physiological pH, thus being able to pass through cell membranes and therefore having better pharmacokinetic properties (El-Kabbani, Ruiz *et al.*, 2004). Regardless of the numerous efforts that have been made in recent decades, to date epalrestat (with a carboxylic acid moiety) is the only ARI that is commercially available (but only in Japan), while fidarestat (with a cyclic imide) has already undergone phase III clinical trials for diabetic neuropathy and was found to be safe, although clinically not very effective. In many cases the failure of new candidates can be attributed to poor pharmacokinetic properties and/or unacceptable side effects (Ramunno *et al.*, 2012). The advantage of the cyclic imide compounds over the carboxylic acids is that they can be uncharged during transport, thus improving their pharmacokinetic properties, and become charged when binding to the enzyme owing to interactions with specific enzyme groups favouring the ionization of the inhibitor (El-Kabbani, Darmanin *et al.*, 2004).

Regarding the selectivity of ARIs with respect to other enzymes of the AKR superfamily, to date the only off-target protein analyzed has been aldehyde reductase (or AKR1A1; Barski *et al.*, 2008; El-Kabbani & Podjarny, 2007; Steuber *et al.*, 2008). Only some recent studies have addressed the selectivity of ARIs *versus* AKR1B10. Gallego *et al.* (2007) reported that tolrestat, an ARI of the carboxylic acid type, inhibited AR-catalyzed and AKR1B10-catalyzed retinaldehyde reduction, and they also resolved the three-dimensional X-ray structure of AKR1B10 in complex with $NADP^+$ and tolrestat. Verma *et al.* (2008) determined the potency of fibrate-mediated inhibition of the carbonyl reduction catalyzed by an AKR1B10 wild-type and C299S mutant, and compared it with the known ARIs zopolrestat, EBPC and sorbinil. They showed that these ARIs followed pure non-competitive inhibition kinetics with AKR1B10. Several recent studies have found new types of AKR1B10 inhibitors that are selective for this enzyme and not for AR: steroids (cholanic acid derivatives, C_{21}-, C_{19}- and C_{18}-steroids), curcuminoids, chromene derivatives, oleanolic acid, some nonsteroidal anti-inflammatory drugs and caffeic acid phenethyl ester (CAPE) derivatives (Fig. 1*a*; Díez-Dacal *et al.*, 2011; Endo, Matsunaga, Kuwata *et al.*, 2010; Endo *et al.*, 2009; Endo, Matsunaga, Soda *et al.*, 2010; Matsunaga *et al.*, 2009; Soda, Hu *et al.*, 2012; Takemura *et al.*, 2011).

In this work, we have screened a series of polyhalogenated ARIs lacking the usual carboxylic acid or cyclic imide moiety through determination of their IC_{50} values against AR and AKR1B10. Some of these compounds have previously been characterized as ARIs (de la Fuente *et al.*, 2003). JF0064 has emerged as a novel lead compound with a new scaffold and its K_i value has been determined for AR and AKR1B10, identifying it as a non-competitive inhibitor. X-ray structures were obtained for both the AR and AKR1B10 holoenzymes with JF0064, observing its binding mode (noting a negatively charged hydroxyl group in the inhibitor) and finding interesting hints for drug design based on this compound. The AR structure highlights the importance of ultrahigh resolution to identify the unexpected protonation state of the inhibitor that is critical for its binding. Hence, overall this work represents another step forward in this topic of pharmacological importance, as AR is a target for antidiabetes intervention and both AR and AKR1B10 have been identified as targets for anticancer therapy (Liu *et al.*, 2009).

Table 1
Data-collection and refinement statistics.

Values in parentheses are for the highest resolution shell.

Protein	AR–$NADP^+$–JF0064	mAKR1B10 K125R/V301L–$NADP^+$–JF0064
Data collection		
X-ray source, beamline	SLS, beamline X06SA	Home source
Wavelength (Å)	0.70849	1.54178
Space group	$P2_1$	$P3_1$
Unit-cell parameters (Å, °)	a = 49.54, b = 66.88, c = 47.53, β = 91.66	a = b = 79.34, c = 50.17
Data-collection temperature (K)	100	100
Resolution range (Å)	30.86–0.85 (0.88–0.85)	23.57–1.75 (1.81–1.75)
No. of observations	1226806	157603
No. of unique reflections	498513	35357
Completeness (%)	93.0 (75.9)	99.0 (94.4)
R_{merge} (%)	3.3 (31.1)†	6.7 (32.6)
Mean $I/\sigma(I)$	23.3 (2.43)	21.9 (2.94)
Multiplicity	2.5 (1.9)	4.5 (2.6)
Model used for MR	1us0	1zua
Refinement statistics		
Resolution range (Å)	30.86–0.85 (0.86–0.85)	23.57–1.75 (1.80–1.75)
R factor (%)	13.48 (22.98)	16.20 (14.76)
R_{free} (%)	14.33 (22.97)	18.64 (17.86)
No. of reflections	498471	35393
No. of reflections (R_{free})	25178	1754
R.m.s.d., bonds (Å)	0.008	0.008
R.m.s.d., angles (°)	1.45	1.31
No. of protein atoms	2787	2671
No. of $NADP^+$ atoms	48	48
No. of JF0064 atoms	22	22
No. of solvent molecules	705	174
Ramachandran plot, residues in (%)		
Favoured regions	98.60	98.77
Allowed regions	1.40	1.23
PDB entry	4igs	4icc

† Anomalous pairs were treated separately.

2. Materials and methods

2.1. Site-directed mutagenesis and purification of recombinant enzymes

The K125R and V301L mutants of AKR1B10 were obtained using wild-type AKR1B10 cDNA cloned into pET30-Xa/LIC (Novagen) as a template. All reactions were performed in a DNA thermal cycler with Phusion High-Fidelity DNA Polymerase (Thermo Scientific). To introduce the V301L mutation, the QuikChange Site-Directed Mutagenesis Kit (Stratagene) method was used with the following primers: GCCTGTAAC**C**TGTTGCAATCC (forward; base pairs 931–951) and ATTGCAACA**G**GTTACAGGCCC (reverse complement; base pairs 929–949). To introduce the

K125R mutation, after the failure of the previous method, a different strategy was used. Two non-overlapping primers were designed covering the AKR1B10 cDNA region from base pairs 393 to 432: TGGGAAAAGGTCATCCCCA (reverse complement; base pairs 393–412) and **G**AGATGA-TAAAGGTAATGCCAT (forward; base pairs 413–434). Mutated nucleotides are shown in bold. After the PCR reaction, phosphorylation and ligation were carried out. The ligation product was incubated with *Dpn*I (New England Biolabs) at 37°C for 60 min to ensure the digestion of the Dam-methylated parental strand. The K125R/V301L double mutant was prepared with pET30-Xa/LIC-AKR1B10 V301L as a template using the same methodology as for the K125R mutation. Finally, in all cases, the resulting nicked circular mutagenic strands were transformed into *Escherichia coli* DH5α and the plasmids were sequenced by GATC Biotech.

The cDNAs of AR and AKR1A1 were cloned into the pET15b plasmid and that of AKR1B10 into the pET16b plasmid (pET30-Xa/LIC was used for the K125R/V301L mutant). AR, wild-type and mutant AKR1B10, and AKR1A1 were recombinantly expressed in the *E. coli* BL21(DE3) strain (Novagen) and were purified using the procedures described previously for AR (Lamour *et al.*, 1999), AKR1B10 (Gallego *et al.*, 2007) and AKR1A1 (Barski *et al.*, 1995). Purity was confirmed by SDS–PAGE and protein concentrations were determined using a NanoDrop ND-1000 (Thermo Scientific).

2.2. Inhibition screening

The IC_{50} activity assays were carried out according to a previously described method (de la Fuente *et al.*, 2003) based on the spectrophotometric quantification of NADPH (ε_{340} = 6220 M^{-1} cm^{-1}) consumption, which takes place when the enzyme catalyzes the reduction of D,L-glyceraldehyde. The assays were performed in 96-well microtitre plates at 25°C in 100 m*M* sodium phosphate buffer pH 7.0 with recombinant protein (AR and AKR1B10), a substrate concentration of about 10 × K_m and 0.2 m*M* NADPH. The final reaction volume was 200 µl per well. The compounds assayed were dissolved in dimethyl sulfoxide (DMSO) and the corresponding solution was added to the well and pre-incubated for 5 min at 25°C prior to addition of the substrate. The final DMSO concentration in the well was 5%(*v*/*v*). The reaction was initiated by the addition of 1, 60 and 5 m*M* glyceraldehyde (for AR, AKR1B10 and AKR1A1, respectively) and the decrease in optical density at 340 nm was monitored for 5 min at 25°C in a microtitre plate reader (Wallace 1420 VICTOR^3, Perkin Elmer). The IC_{50} value for each test compound was determined as the compound concentration that inhibits enzymatic activity by 50%. The IC_{50} was calculated using the *GraFit* program (v.5.0; Erithacus Software) and values were given as the mean ± standard deviation of three experiments.

2.3. Determination of K_i values

The inhibition pattern and K_i values were determined by using six different concentrations of D,L-glyceraldehyde as a substrate and three concentrations of JF0064 inhibitor: 0.3, 0.6 and 1.8 µ*M* for AR and 0.5, 1 and 3 µ*M* for AKR1B10. The enzymatic activity was monitored by the change in NADPH concentration (absorbance at 340 nm) at 25°C in a UV–visible spectrophotometer (Cary 400 Bio, Varian) using a reaction mixture containing 0.1 *M* sodium phosphate pH 7.4 and 0.5 m*M* NADPH. The final concentration of carrier solvent, DMSO, was 5%(*v*/*v*). One unit (U) of activity corresponds to the transformation of 1 µmol substrate per minute. The kinetic constants were calculated by fitting the initial rates to the appropriate equation using *GraFit* (v.5.0; Eritacus Software). The K_i values are expressed as the mean ± standard deviation of three independent determinations.

2.4. Crystallization and structure determination

Regarding the AR–NADP$^+$–JF0064 complex, crystals could not be obtained by co-crystallization. Therefore, an initial soaking trial with crystals of native AR–NADP$^+$ obtained under the published conditions (50 m*M* ammonium citrate pH 5.0, 20% polyethylene glycol, PEG 6000) was performed with 10 m*M* JF0064 for 6 d at 24°C without success. To avoid interference with the citrate used during crystallization, the ammonium citrate was replaced by MES. Crystals of native AR–NADP$^+$ were obtained in 50 m*M* MES pH 5.5, 20 m*M* ammonium sulfate, 20% PEG 6000 by the hanging-drop vapour-diffusion method at 24°C. With the aim of obtaining electron density for JF0064, a second trial of soaking was performed on these crystals with 4 m*M* JF0064 for 6 d at 24°C. Cryocooling in liquid nitrogen was carried out using a cryoprotecting solution containing 40% PEG 6000. Data collection was performed to 0.85 Å resolution on the X06SA beamline at the Swiss Light Source. The crystals belonged to space group $P2_1$, with one protein molecule in the asymmetric unit. Data were processed with *HKL*-2000 (Otwinowski & Minor, 1997). Data-collection statistics are listed in Table 1.

Regarding the AKR1B10–NADP$^+$–JF0064 complex, reductive methylation of lysine residues was performed to improve the crystal packing. The method used is derived from that published previously (Rayment, 1997; Rayment *et al.*, 1993). After protein purification, the methylation reaction was performed overnight in 50 m*M* HEPES pH 8.0 at a protein concentration of 1 mg ml^{-1}. 50 µl freshly prepared 1 *M* dimethylamine–borane complex (Sigma–Aldrich) and 80 µl 1 *M* formaldehyde were added per millitre of protein solution and incubated at 4°C for 16 h. Methylation was stopped by the addition of 25 m*M* Tris–HCl pH 8.0. Prior to crystallization, methylated AKR1B10 (mAKR1B10) was dialyzed against 20 m*M* NaCl, 25 m*M* Tris pH 8.0, 40 m*M* HEPES pH 8.0, concentrated to 30 mg ml^{-1} and then mixed with a solution of NADP$^+$ to achieve a 1:4 molar ratio of AKR1B10:NADP$^+$. For the co-crystallization with JF0064, a 4 m*M* inhibitor concentration was used. Crystals of the complex were obtained by the hanging-drop vapour-diffusion method at 24°C. The protein solution was mixed with an equal volume of precipitating solution consisting of 100 m*M* sodium cacodylate pH 9.0, 30% PEG 6000 and equilibrated against 500 µl of the precipitating solution. The same crystallization conditions were used for

wild-type mAKR1B10 and the mAKR1B10 K125R and mAKR1B10 K125R/V301L mutants. Cryocooling in liquid nitrogen was carried out using a cryoprotecting solution containing 40% PEG 6000. X-ray data for mAKR1B10 K125R/V301L–NADP$^+$–JF0064 were collected on the home laboratory X-ray source to 1.75 Å resolution. The data were processed with *HKL*-2000 (Otwinowski & Minor, 1997). Data-collection statistics are listed in Table 1.

2.5. Structural refinement

The atomic coordinates of the human AR–NADP$^+$–IDD594 complex (PDB entry 1us0; Howard *et al.*, 2004), which is the highest resolution AR structure available, were used to solve the structure of the AR ternary complex, while those of AKR1B10–NADP$^+$–tolrestat (PDB entry 1zua; Gallego *et al.*, 2007) were used for AKR1B10. In both cases, molecular replacement was performed with *AMoRe* (Navaza, 2001). Crystallographic refinement involved repeated cycles of conjugate-gradient energy minimization and temperature-factor refinement performed with *REFMAC*5 (Murshudov *et al.*, 2011) and *PHENIX* (Adams *et al.*, 2010). The JF0064 PDB file was built using *ChemDraw* (Perkin Elmer) to generate a two-dimensional formula and was refined with *ChemBio3D* (Perkin Elmer) to add the stereochemistry and with *Open Babel* (O'Boyle *et al.*, 2011) for conversion to PDB format. The restraint dictionary (libcif format) was then written with *REFMAC*5 based on the PDB and mtz files, with standard stereochemistry. Amino-acid side chains and water molecules were fitted into $2F_o - F_c$ and $F_o - F_c$ electron-density maps with *Coot* (Emsley *et al.*, 2010). The final $F_o - F_c$ map indicated clear electron density for JF0064 in both complexes. Refinement statistics are presented in Table 1. The atomic coordinates have been deposited in the PDB (entries 4igs and 4icc) and will be released immediately upon publication. Finally, in order to perform a more complete study regarding the fine geometric details of the ultrahigh-resolution AR–NADP$^+$–JF0064 structure, the *SHELXL* program (Sheldrick, 2008) was used. A `.lst` file corresponding to JF0064 distances and angles is included within the Supporting Information[1]. Related figures were prepared with *PyMOL* (v.1.3; Schrödinger).

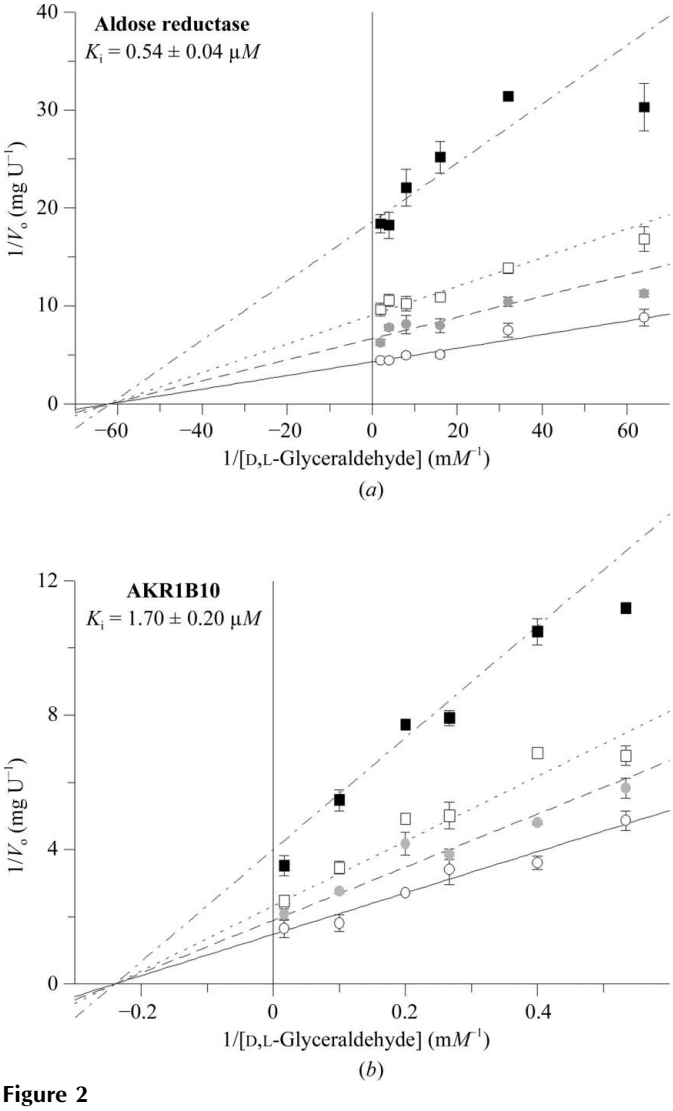

Figure 2
Inhibitory effect of JF0064 on the glyceraldehyde reductase activity of AR and AKR1B10. (*a*) Lineweaver–Burk plot showing the effect on the reduction of D,L-glyceraldehyde by AR at different JF0064 concentrations: 0 (empty circles), 0.3 µ*M* (filled circles), 0.6 µ*M* (empty squares) and 1.8 µ*M* (filled squares). (*b*) Lineweaver–Burk plot showing the effect on the reduction of D,L-glyceraldehyde by AKR1B10 at different JF0064 concentrations: 0 (empty circles), 0.5 µ*M* (filled circles), 1 µ*M* (empty squares) and 3 µ*M* (filled squares). Abbreviations: U, units (µmol min^{-1}), V_o, initial rate. Data fitting and plots were performed with *GraFit* (v.5.0; Erithacus Software).

Table 2
IC_{50} values of the JF inhibitor series against AR and AKR1B10.

Compound	IC_{50} (µ*M*) AR	IC_{50} (µ*M*) AKR1B10	IC_{50} ratio AKR1B10/AR
1†	6.4 ± 1.1‡	—	—
2†	25%‡	—	—
3†	0%‡	—	—
JF0021	3.2 ± 1.1	32 ± 4	10
JF0025 (**15**†)	5.7 ± 1.6	2.3 ± 0.2	0.4
JF0042 (**24**†)	8.9 ± 4.2	>55	>6.2
JF0053 (**27**†)	4.4 ± 2.5	3.4 ± 0.5	0.8
JF0064	0.3 ± 0.1	1.0 ± 0.1	3.4
JF0127	3.7 ± 1.6	1.6 ± 0.2	0.4
JF0143	6.5 ± 4.5	1.8 ± 0.2	0.3
JF0246 (**13**†)	>46	>200	—

† Compounds named as in de la Fuente *et al.* (2003). ‡ Data taken from de la Fuente *et al.* (2003): IC_{50} value or percentage of inhibition at 25 µg ml^{-1} compound.

2.6. Molecular dynamics

The molecular-dynamics (MD) simulations of AKR1B10–NADP$^+$–JF0064 were performed using *Amber*12 and the SPFP precision model (Le Grand *et al.*, 2013). Analysis of the trajectory was carried out using *ptraj* and *cpptraj* (Roe & Cheatham, 2013) as implemented in *AmberTools*12 (Case *et al.*, 2012; Salomon-Ferrer *et al.*, 2013). Molecular preparation of the AKR1B10 holoenzyme–JF0064 complexes was carried

[1] Supporting information has been deposited in the IUCr electronic archive (Reference: RR5047).

out using *MOE* (v.2012.10; Chemical Computing Group, Montreal, Canada; http://www.chemcomp.com). The input structures of the protein and the ligand were prepared from the mAKR1B10 K125R/V301L–NADP$^+$–JF0064 structure reported here; for the wild-type structure residues Arg125 and Leu301 were mutated to Lys125 and Val301 *in silico* using *MOE*. For AKR1B10 and AKR1B10 K125R/V301L, each in complex with JF0064, 110 ns MD simulations were carried out (for the ligand with protonated hydroxyl groups and the ligand containing the deprotonated hydroxyl group at position 4). Further details of the procedure are included in the Supporting Information. Related figures were prepared with *PyMOL* (v.1.3; Schrödinger).

3. Results

3.1. Determination of the selectivity of the JF inhibitor series for AR and AKR1B10

In a previous study, de la Fuente *et al.* (2003) discovered a polybrominated diaryl ether in a marine sponge (compound **1** in Fig. 1*b*) which was found to inhibit recombinant human

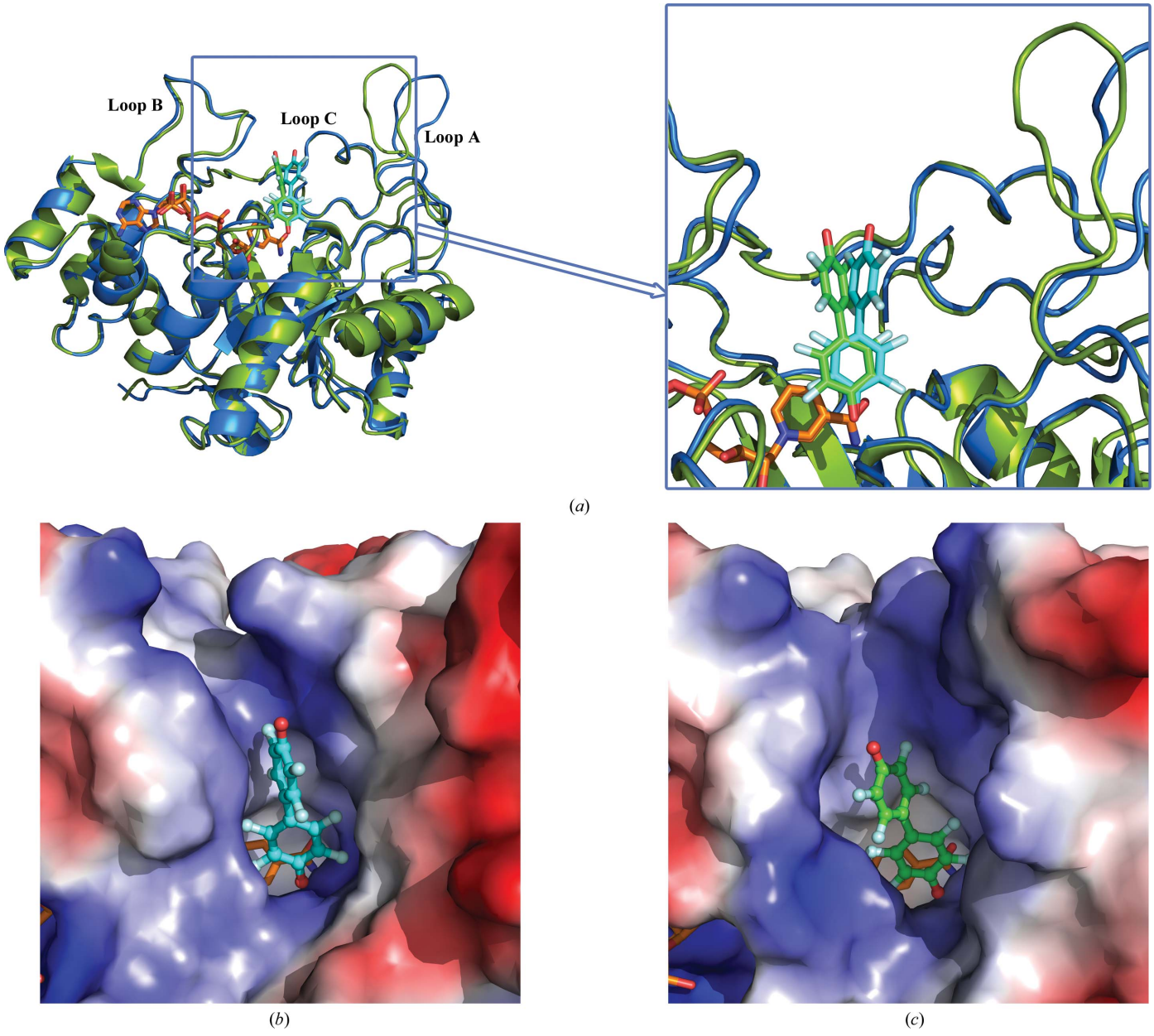

Figure 3
General view of the X-ray structures of the AR–NADP$^+$–JF0064 and mAKR1B10 K125R/V301L–NADP$^+$–JF0064 complexes. (*a*) Superposition of the AR–JF0064 and mAKR1B10–JF0064 complexes with the protein main chain represented as cartoon loops (AR, marine blue; mAKR1B10, olive green) and the cofactor NADP$^+$ (orange) and JF0064 as sticks (AR, cyan; mAKR1B10, green). External loops are highlighted and an enlargement of the JF0064 binding site is shown inside the square. (*b*, *c*) JF0064 complexed with AR (*b*) or mAKR1B10 K125R/V301L (*c*) holoenzyme in a surface representation coloured according to the local electrostatic potential (blue, positive charge; white, neutral; red, negative charge) calculated with *PyMOL*.

AR with an IC_{50} value of 6.4 μM. Two other natural polybrominated diaryl ethers (compounds **2** and **3** in Fig. 1*b*) isolated from the same species and closely related to **1** were also assayed. Thus, a series of polyhalogenated analogues (Fig. 1*b*) were synthesized and tested *in vitro* to explore the structure–activity relationship (SAR) and displayed various degrees of inhibitory activity (de la Fuente *et al.*, 2003). In the present study, four of these compounds and four other unpublished polyhalogenated derivatives were analyzed with respect to their IC_{50} values against AR and AKR1B10 to find new and selective inhibitors of these enzymes (Fig. 1*b*, Table 2). JF0064 was detected to be the most potent compound with both AR and AKR1B10 (IC_{50} for AR = 0.3 ± 0.1 μM; IC_{50} for AKR1B10 = 1.0 ± 0.1 μM). In order to assess the selectivity of JF0064 in comparison to AKR1A1, we determined its IC_{50} against the latter enzyme. The value obtained was 7.4 ± 0.6 μM, which represents about 25-fold and sevenfold selectivity for AR and AKR1B10, respectively.

3.2. Determination of the K_i values of the novel type of ARI JF0064

Once the IC_{50} assays had revealed a new lead among the screened compounds, determination of the K_i value and the inhibition mechanism was performed for JF0064. This compound represents a novel inhibitor chemical class, as it contains neither the carboxylic acid nor the cyclic imide moiety incorporated in most ARIs and AKR1B10 inhibitors. In general, these inhibitors display a characteristic non-competitive inhibition pattern against the substrate (Barski *et al.*, 2008; Bohren & Grimshaw, 2000; Verma *et al.*, 2008).

For the determination of K_i values, D,L-glyceraldehyde was used as a substrate with both AR and AKR1B10. JF0064 inhibition followed a non-competitive pattern with both enzymes (Fig. 2), showing values of 0.54 and 1.7 μM for AR and AKR1B10, respectively. Consequently, although JF0064 belongs to a novel ARI/AKR1B10 inhibitor chemical class, it is likely to follow the same inhibition mechanism. These data suggest an acidic character of the tetrafluorophenol moiety in JF0064, similar to that of cyclic imides, *i.e.* the inhibitor is transported as a neutral molecule and becomes negatively charged when binding to the target enzyme.

3.3. Structure determination of AR and AKR1B10 complexes with JF0064 by X-ray crystallography

Following the IC_{50} assays, JF0064 was selected for protein crystallization trials with both AR and AKR1B10 with the purpose of finding (i) the structural basis of the inhibition properties of this new scaffold and (ii) some hints for increasing its potency and selectivity.

Regarding the AR–$NADP^+$–JF0064 complex, crystals could not be obtained by co-crystallization. A first soaking trial was performed with crystals of native AR–$NADP^+$ obtained under the published conditions (Lamour *et al.*, 1999) in ammonium citrate buffer pH 5.0. The X-ray structure obtained displayed

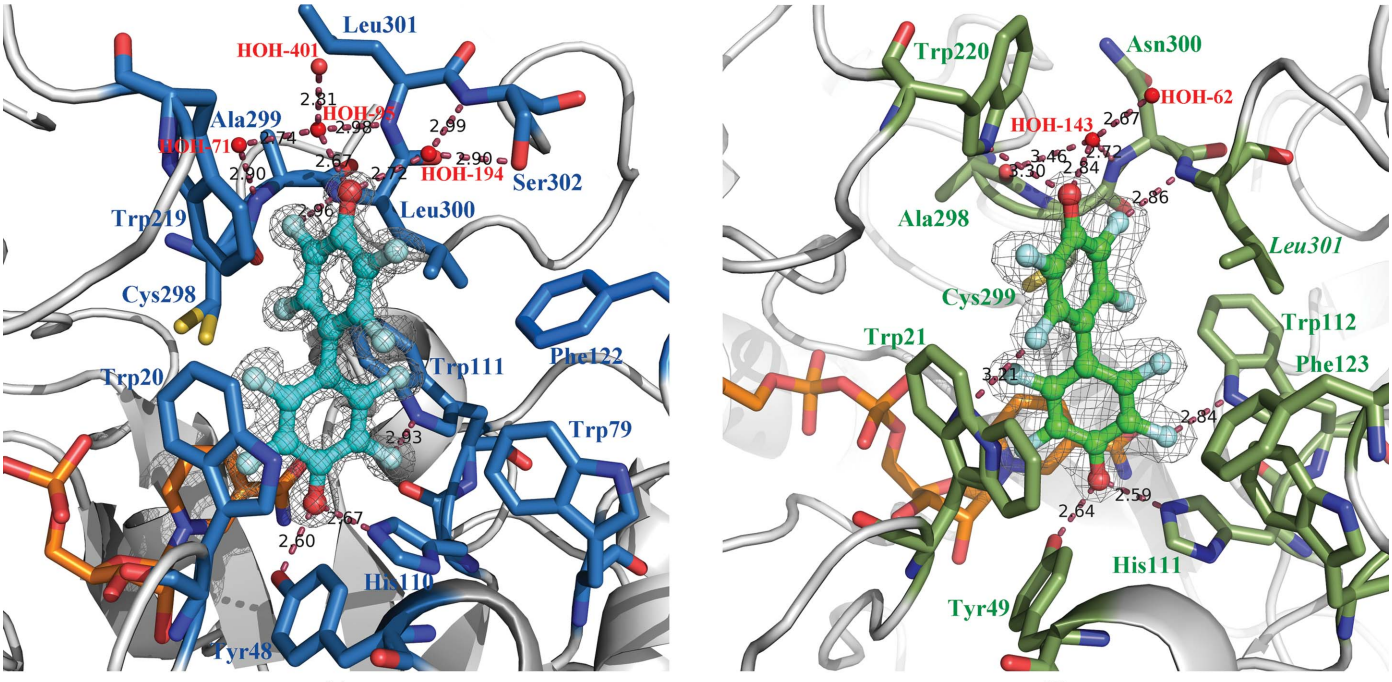

Figure 4
Inhibitor-binding site of AR/AKR1B10–JF0064 complexes. (*a*) Atomic representation of the inhibitor-binding site for the AR–$NADP^+$–JF0064 complex, with the inhibitor electron density shown as a σ_A-weighted $2F_o - F_c$ map contoured at the 2σ level. Water molecules HOH-95, HOH-194 and HOH-245 (not shown for clarity) are hydrogen bonded to the JF0064 outer hydroxyl group. (*b*) Atomic representation of the inhibitor-binding site for the mAKR1B10 K125R/V301L–$NADP^+$–JF0064 complex with the inhibitor electron density shown as a σ_A-weighted $2F_o - F_c$ map contoured at the 1σ level. Protein main chain is represented with white cartoon loops and key residues forming the JF0064-binding site are displayed as sticks, while the inhibitor is shown in ball-and-stick representation. The mutated Leu301 is identified with a label in italics. The colour code is as in Fig. 3, water molecules are represented as red spheres and labels are in the corresponding colours. Distances are indicated in Å for hydrogen-bonded atoms.

low-quality electron density for the JF0064 molecule (data not shown). Citrate is an uncompetitive inhibitor of AR, and the X-ray structure of the native crystals showed two citrate molecules bound in the active site of the protein (Biadene *et al.*, 2007; Harrison *et al.*, 1994), which could potentially hamper JF0064 binding. Since pig AR had been crystallized in the presence of MES buffer pH 6.2, we used this buffer instead of ammonium citrate (Calderone *et al.*, 2000; Urzhumtsev *et al.*, 1997). Crystals of native AR–NADP$^+$ obtained in 50 m*M* MES pH 5.5 were used for a second trial of soaking with compound JF0064. The X-ray structure was determined at 0.85 Å resolution and refined to a final R_{work} of 13.48% and R_{free} of 14.33%. The structure of the complex was determined in space group $P2_1$, which is the most commonly observed for AR crystals. There was one monomer in the asymmetric unit, with a calculated solvent content of 44.00% and a Matthews coefficient of 2.20 Å^3 Da^{-1}. Table 1 shows the data-collection and refinement statistics.

Regarding AKR1B10, holoenzyme or ternary-complex crystals could not be obtained using the wild-type or several mutant proteins, including active-site and surface mutants. Attempts failed under the published conditions and with robotic crystallization screens, except for tolrestat-containing complexes. Indeed, crystals of AKR1B10–NADP$^+$–tolrestat and of AKR1B10 V301L–NADP$^+$–tolrestat complexes were obtained.

Several studies have demonstrated that methylation of the solvent-exposed ε-amino group of lysine residues changes the properties of the protein and may promote crystallization *via* improvement of crystal packing (Sledz *et al.*, 2010; Walter *et al.*, 2006). Therefore, reductive methylation of wild-type AKR1B10 was assayed prior to crystallization trials. Crystals of methylated AKR1B10 (mAKR1B10) holoenzyme were obtained under the conditions previously published for the AKR1B10–NADP$^+$–tolrestat complex (Gallego *et al.*, 2007), and its X-ray structure revealed that Lys125 in loop A was monomethylated (data not shown). Thus, with the aim of retaining the positive charge, this residue was mutated to arginine. Co-crystals were obtained using the mAKR1B10 K125R–NADP$^+$–JF0064 complex, but they did not show electron density corresponding to the bound ligand (data not shown). However, when including the V301L mutation, the X-ray structure of an mAKR1B10 K125R/V301L–NADP$^+$–JF0064 complex co-crystal was obtained at 1.75 Å resolution and refined to a final R_{work} of 16.20% and R_{free} of 18.64%. The structure of the complex was determined in space group $P3_1$. There was one monomer in the asymmetric unit, with a calculated solvent content of 50.67% and a Matthews coefficient of 2.49 Å^3 Da^{-1}. Table 1 shows the data-collection and refinement statistics.

Prior to crystallization trials of wild-type and mutant forms of mAKR1B10, they were tested for activity using an enzymatic assay. In all cases, the specific activity of the mAKR1B10 forms was the same as that of wild-type AKR1B10 ($\sim$0.8 µmol min^{-1} mg^{-1} with glyceraldehyde, as reported previously; Gallego *et al.*, 2006), ensuring that the methylated proteins kept their functionality. JF0064 IC_{50} assays were also performed with AKR1B10 K125R/V301L and mAKR1B10 K125R/V301L, showing very similar values (7 $\pm$ 1.7 and 8.2 $\pm$ 1.1 µ*M*, respectively) and ensuring that the methylated protein behaved similarly in inhibition assays.

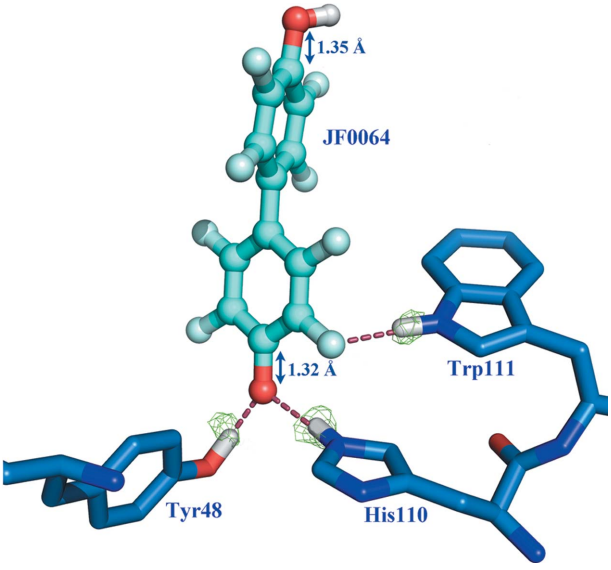

Figure 5
Detail of the inhibitor-binding site of the AR–NADP$^+$–JF0064 complex at ultrahigh resolution: side view of an atomic model of JF0064 in cyan ball-and-stick representation with the AR interacting residues Tyr48, His110 and Trp111 shown as marine blue sticks. H atoms of these residues which are involved in hydrogen bonds are displayed in sticks and their electron densities are shown as σ_A-weighted $F_o - F_c$ maps contoured at the 1.5σ level in green. The length of the C—O bond of each phenol moiety of JF0064 is indicated.

3.4. Structure overview and inhibitor-binding site of the AR/AKR1B10–NADP$^+$–JF0064 complexes

The X-ray structures of both complexes revealed an $(\alpha/\beta)_8$ barrel characteristic of the proteins of the AKR superfamily. The NADP$^+$ is bound in an extended conformation adjacent to the active site located at the C-terminal end of the barrel, with the inhibitor JF0064 positioned between the external loops B and C. JF0064 is a symmetrical molecule composed of two identical phenol rings linked by a single C—C bond. Each ring contains four F atoms in the *ortho* and *meta* positions and the hydroxyl group in the *para* position (Figs. 1*b* and 1*c*). In the enzyme–inhibitor complexes, one of the rings (the 'inner ring') is bound to the anion-binding pocket, while the other ring (the 'outer ring') points towards the solvent and is near loops B and C (Fig. 3). Comparison of the binding modes of JF0064 between AR and AKR1B10 shows that while the inner ring is similarly placed but slightly rotated, the outer ring is significantly displaced (Fig. 3*a*). In this regard, it is noteworthy that while the binding of JF0064 does not open the specificity pocket in either of the two structures, there are some differences between the two active-site binding pockets given by the different positioning of the three external loops (Fig. 3).

The analysis of interactions between the AR holoenzyme and JF0064 (Figs. 4*a* and 5) shows that catalytic residues Tyr48

and His110 establish hydrogen bonds to the O atom of the hydroxyl group of the inner ring (2.60 and 2.67 Å, respectively) and define the prototypical anion-binding pocket observed in the AR–ARI complexes. Moreover, this hydroxyl

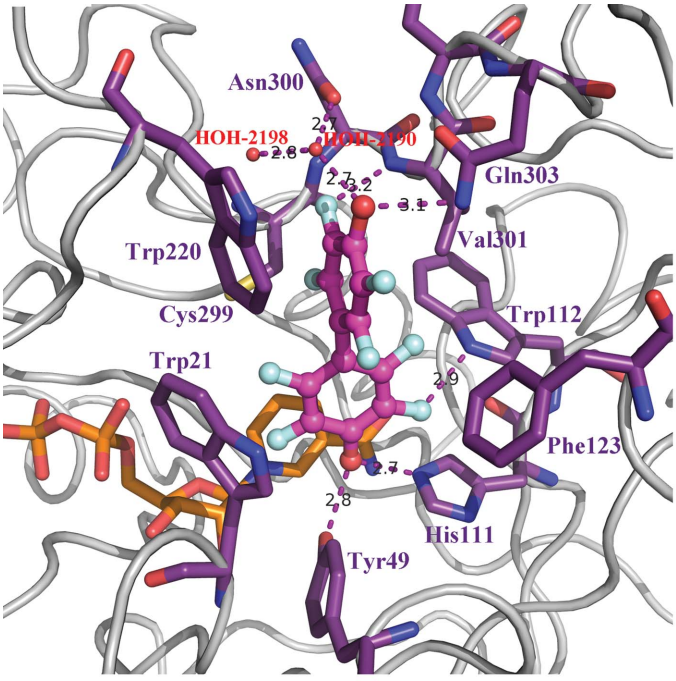

(*a*)

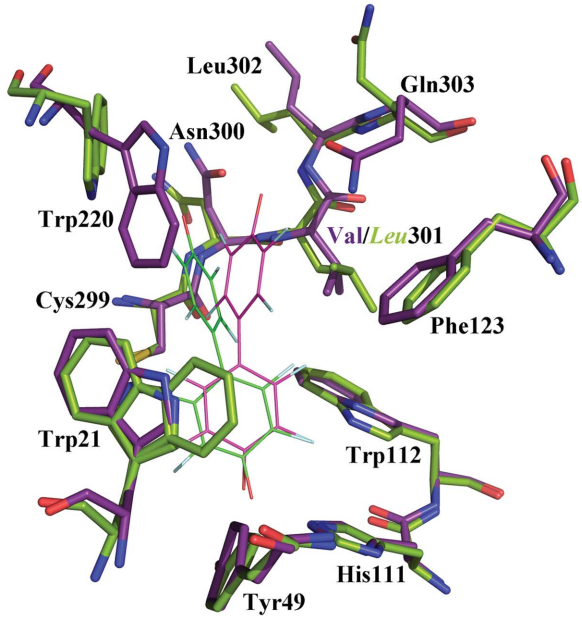

(*b*)

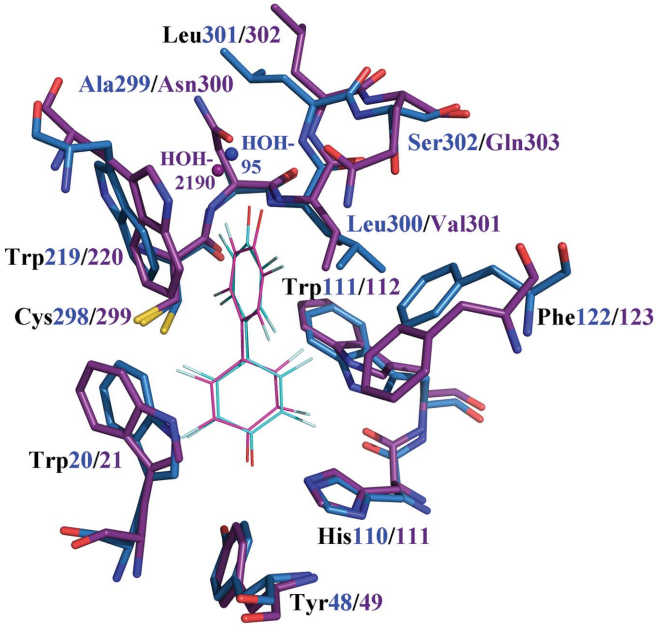

(*c*)

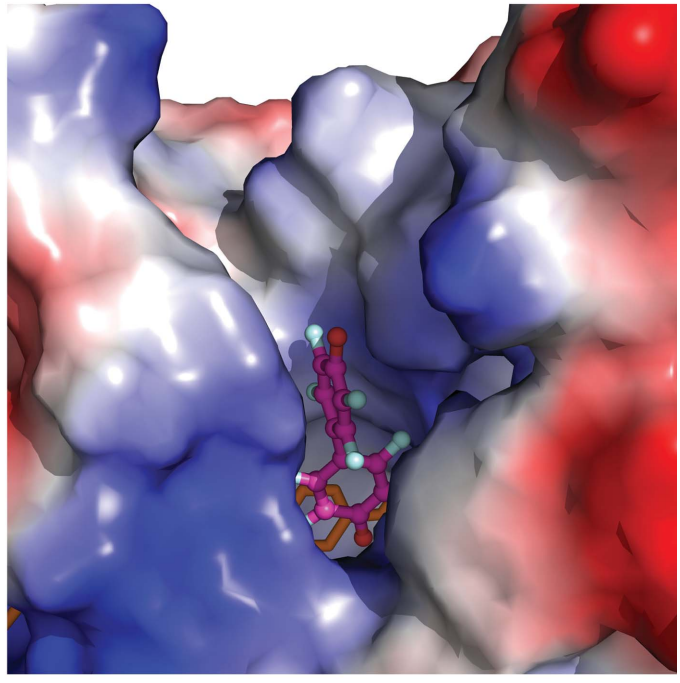

(*d*)

Figure 6
Molecular-dynamics (MD) simulation of the AKR1B10 wild-type holoenzyme complex with JF0064 and comparison with the mAKR1B10 mutant and AR crystallographic structures. The presented MD frame was derived from clustering of the second 110 ns MD run of this protein complex. The shown cluster is populated with 5849 frames (53.2% of this MD run). (*a*) Atomic representation of the inhibitor-binding site for the complex of the wild-type AKR1B10 holoenzyme with JF0064. Protein main chain is represented by white cartoon loops and key residues forming the JF0064-binding site are displayed as violet sticks, while the inhibitor is shown in pink ball-and-stick representation and the cofactor in shown as orange sticks. (*b*) Atomic representation of the inhibitor-binding site residues of the mAKR1B10 K125R/V301L–NADP$^+$–JF0064 complex (olive green sticks) superimposed onto the AKR1B10–NADP$^+$–JF0064 complex (violet sticks). Inhibitor molecules are shown as thinner green and pink sticks. Residue labels are shown in black, except for the case of the mutated residue Leu301, where they are shown in olive green italics. (*c*) Atomic representation of the inhibitor-binding site residues of the AKR1B10–NADP$^+$–JF0064 complex (violet sticks) superimposed onto AR–NADP$^+$–JF0064 (blue sticks). Inhibitor molecules are shown as thinner pink and cyan sticks. Residue labels are in violet for AKR1B10 and in blue for AR. (*d*) JF0064 (pink ball-and-stick representation) complexed with AKR1B10 holoenzyme in a surface representation coloured according to the local electrostatic potential (blue, positive charge; white, neutral; red, negative charge) calculated with *PyMOL*.

group seems to be negatively charged, which is supported by two different observations. Firstly, its observed C—O bond distance is 1.3229 ± 0.0124 Å (obtained by an unrestrained refinement with *SHELXL*; Supporting Information), which is significantly shorter than the C—OH bond distance reported as 1.36 Å (Prince *et al.*, 2006). On the contrary, the distal ring hydroxyl group presents a C—O bond distance of 1.3528 ± 0.0189 Å (obtained by an unrestrained refinement with *SHELXL*; Supporting Information), indicating that it is not charged. The second observation supporting the negative charge of the inner ring hydroxyl group is the observation of difference map peaks corresponding to the H atoms bonded to the OH of Tyr48 and the $N^{\varepsilon 2}$ atom of His110 (green contours in Fig. 5). The H atom of the distal ring hydroxyl group of JF0064 is not observed in the difference map (at the same contour level as for the inner ring hydroxyl), possibly because this hydroxyl is exposed to the solvent. Trp111 forms a hydrogen bond to the F3 atom (2.93 Å; Figs. 4*a* and 5) and also makes a hydrophobic contact with the inner ring, along with Trp20 and the nicotinamide ring of the cofactor. The outer ring interacts through hydrophobic contacts with Trp219, Leu300 and Cys298, and with a hydrogen-bond network involving its hydroxyl group, water molecules HOH-71, HOH-95, HOH-194 and the main-chain N atoms of residues Ala299, Leu301 and Ser302 (and the side-chain O atom of Ser302). HOH-245 also interacts with the hydroxyl of the outer ring and other water molecules, but it is not bonded to the protein. Moreover, an additional hydrogen bond is formed between the N atom of the main chain of Leu300 and the F3′ atom. All of these contacts and their corresponding distances can be observed in Fig. 4(*a*).

The analysis of the interactions between the mAKR1B10 K125R/V301L holoenzyme and JF0064 (Fig. 4*b*) shows that, analogously to its AR counterpart, the catalytic residues Tyr49 and His111 establish hydrogen bonds to the acidic hydroxyl of JF0064 (2.64 and 2.59 Å, respectively), while Trp112 interacts with F3 (2.84 Å). Trp21, Trp112 and the nicotinamide moiety of $NADP^+$ also make hydrophobic interactions with the inhibitor inner ring. In contrast, the side-chain $N^{\varepsilon 1}$ atom of Trp21 in the *B* conformation (40% occupancy) forms a hydrogen bond to F2′ (3.21 Å). Regarding the outer ring, the hydroxyl group of the inhibitor interacts through hydrogen bonds with the $N^{\varepsilon 1}$ atom of Trp220 and HOH-143. This water molecule, in turn, extends the hydrogen-bond network to the carbonyl O atom of Ala298 and to the main-chain N atom of Asn300. Finally, the F5′ atom is hydrogen-bonded to the main-chain N atom of Leu301 (2.86 Å). All of these contacts and their corresponding distances can be observed in Fig. 4(*b*).

3.5. Molecular dynamics and inhibitor-binding site of wild-type AKR1B10

As the structure of wild-type AKR1B10 holoenzyme complexed with JF0064 could not be determined, we decided to perform molecular dynamics (MD) in order to simulate the inhibitor-binding pose based on the crystal structure of mAKR1B10 K125R/V301L. Regarding the AKR1B10 wild-type complex, MD could only achieve a binding geometry of the ligand that closely approaches the state in the crystal structure when the ligand was deprotonated at the inner hydroxyl group. In this case, we obtained an r.m.s.d. value close to 1 Å from the crystal structure (see the r.m.s.d. plots in the Supporting Information). In the case in which the inner hydroxyl group had been protonated, we only obtained r.m.s.d.s of around 2 Å or higher (data not shown). On the other hand, the outer tetrafluorophenol moiety is more flexible as it is more strongly exposed to the solvent and to flexible external loops. The inhibitor-binding site in the wild-type protein is similar to that in the crystal structure for the inner tetrafluorophenol moiety. The previously described main contacts between JF0064 and residues Tyr49, His111 and Trp112 remain conserved (Fig. 6*a*). Superimposition of the X-ray structure and a representative MD pose (see Supporting Information) shows that the most significant change is indeed the replacement of Leu301 by Val (Arg125 is located far from the pocket and should not be involved in JF0064 binding). Val301 cannot provide a proper stacking with Trp112 as does Leu; accordingly, Val301 is quite mobile. The flexibility of Val301 allows Gln303 to shift closer to the inhibitor, while the upper ring of JF0064 can approach closer to loop C (Fig. 6*b*). These movements finally allow the formation of a hydrogen bond between the outer hydroxyl and the N atom of the amide of Gln303, a direct interaction that is not observed in the X-ray mAKR1B10 mutant structure (Figs. 4*b* and 6*b*). This is consistent with a lower IC_{50} value for wild-type AKR1B10 (1.0 μ*M versus* 8.2 μ*M* for the mutant).

4. Discussion

4.1. Structural basis for the inhibitory potency and selectivity of the JF0064 lead compound

While nearly 100 X-ray structures of AR have been deposited in the PDB, only two structures had been released for AKR1B10 prior to the submission of this publication (during the revision procedure, a study including four new AKR1B10 X-ray structures was published; Zhang *et al.*, 2013): (i) a ternary complex with tolrestat (PDB entry 1zua; Gallego *et al.*, 2007) and (ii) a ternary complex with fidarestat (PDB entry 4gab; recently solved in our laboratory by replacement soaking; Ruiz *et al.*, 2013). This reflects the intrinsic difficulties in obtaining crystals of AKR1B10–ligand complexes.

The majority of methods used to overcome these difficulties are focused on changing the crystallization conditions. However, the properties of the protein molecule also strongly influence the crystallization process. Thus, an alternative approach is to modify the macromolecule rather than the crystallization conditions. The surface lysine methylation (SLM) technique provides such a modification and can improve the rate of success of protein crystallization by chemically methylating lysine residues. SLM promotes crystallization as the methylation of the solvent-exposed ε-amino group of lysines changes some of the protein properties (pI, solubility and hydropathy) and decreases the surface entropy

Table 3
Hydrogen-bond interactions of inhibitors containing hydroxyl groups in the active site of AR/AKR1B10.

All the interactions were predicted from computer docking simulations, with the exception of those of JF0064 in aldose reductase and the same inhibitor with residues Tyr49 and His111 in AKR1B10.

	Residues in hydrogen-bond interactions (chemical groups involved)		
Inhibitor	Anion-binding pocket	Specificity pocket†	Reference
AR			
JF0064	Tyr48/His110 (hydroxyl)	No interaction	Present work
Benzopyran-4-one derivatives	Tyr48/His110 (hydroxyl)	Thr113 (hydroxyl)	Costantino *et al.* (1999), Rastelli *et al.* (2000)
Chalcone derivative	Tyr48/His110 (hydroxyl)	Thr113 (hydroxyl)	Rastelli *et al.* (2000)
AKR1B10			
JF0064	Tyr49/His111 (hydroxyl)	Gln303 (hydroxyl)	Present work
Caffeic acid‡	Tyr49/His111 (hydroxyl)	Gln114 (hydroxyl)	Soda, Hu *et al.* (2012)
Mangostin	His111 (hydroxyl)	Gln303 (hydroxyl)	Soda, Endo *et al.* (2012)
Isolithocholic acid	Tyr49/His111 (hydroxyl)	Lys125/Gln303 (carboxyl)	Endo *et al.* (2009)
Bisdemethoxycurcumin	Tyr49/His111 (hydroxyl)	Gln114/Ser304 (hydroxyl)	Matsunaga *et al.* (2009)
Oleanolic acid	Tyr49/His111 (hydroxyl)	Gln303 (carboxyl)	Takemura *et al.* (2011)
MTF§	Trp21/His111 (hydroxyl/carbonyl)	Lys125/Gln303 (hydroxyl)	Zhao *et al.* (2010)
Glycyrrhetic acid	Tyr49/His111 (hydroxyl)	Lys125 (carboxyl)	Endo, Matsunaga, Soda *et al.* (2010)
Ursolic acid	Tyr49 (hydroxyl)	Lys125 (carboxyl)	Takemura *et al.* (2011)

† The listed interactions mostly open the specificity pocket. When this does not happen, the residues interacting with the inhibitor indicated here are outside the anion-binding pocket. ‡ Caffeic acid phenethyl ester (CAPE)-based inhibitor: 3-(4-hydroxy-2-methoxyphenyl)acrylic acid 3-(3-hydroxyphenyl)propyl ester. § 9-Methyl-2,3,7-trihydroxy-6-fluorone.

(Kim *et al.*, 2008; Sledz *et al.*, 2010; Walter *et al.*, 2006). In the present work, SLM allowed co-crystals to be obtained after numerous trials of crystallization conditions with the wild-type and mutant proteins.

In addition to SLM, two amino-acid mutations were introduced. The first one was the replacement of Lys125 by an Arg residue. This lysine is monomethylated after SLM; however, Lys125 is in a key position and therefore could presumably be involved in interactions with some of the inhibitors (Table 3; Endo, Matsunaga, Kuwata *et al.*, 2010; Endo *et al.*, 2009; Matsunaga *et al.*, 2009; Soda, Hu *et al.*, 2012; Takemura *et al.*, 2011; Zhao *et al.*, 2010) and probably in the loop A conformation. Indeed, the most mobile region in the AKR1B10 holoenzyme complex with tolrestat was loop A, extending from Lys125 to Ala131 (Gallego *et al.*, 2007). Therefore, in order to keep the positive charge, this lysine was mutated to arginine. The other mutation was the exchange of Val301 to Leu (the corresponding residue in AR). In fact, co-crystal preparation was attempted with mAKR1B10 K125R–JF0064, but no electron density could be observed for the ligand. As we reported previously in the case of the AKR1B10 V301L–$NADP^+$–fidarestat complex (Ruiz *et al.*, 2013), the mutation of Val301 to Leu is an essential prerequisite for the observation of JF0064 by X-ray crystallography. While in the complex with fidarestat this fact can be explained by the stronger binding of the inhibitor, in the present case it is not very evident (it could be linked to loop A rearrangement originating from the V301L mutation).

A structural biology highlight of the present work is the ultrahigh resolution (1 Å or better; Lecomte *et al.*, 2008) of the AR–$NADP^+$–JF0064 ternary complex, which was determined at 0.85 Å. At such resolution, the level of detail observed in the best-ordered areas approaches that in small-molecule studies. H atoms and bond densities are clearly visible and estimation of the atomic charges starts to be possible (Podjarny *et al.*, 2004). In this sense, the ultrahigh resolution has unveiled some important structural and biochemical details regarding the interaction of JF0064 with AR and its inhibition. The most remarkable observation is the evidence that JF0064 is negatively charged. Firstly, the observed C—O bond distance of the hydroxyl group of the inner ring (1.32 Å) fits that of a charged hydroxyl group, while in the case of the hydroxyl group of the distal ring (1.35 Å) it matches a non-charged group better. Interestingly, Gregson and coworkers have obtained the three-dimensional structure of *meso*-5,5,7,12,12,14-hexamethyl-1,4,8,11-tetraazacyclotetradecane: 4,4′-biphenol (1:2 molar ratio), a salt containing both neutral and anionic biphenol units (Gregson *et al.*, 2000). They observed that the distances for the two uncharged C—OH bonds were 1.358 and 1.360 Å, whereas in the case of the charged C—O bond the distance was 1.337 Å; a change in the same direction is observed in this work. Secondly, it is possible to observe the H atoms of the hydrogen-bonded residues Tyr48 and His110 in the difference maps (Fig. 5). Indeed, Costantino *et al.* (1999) measured the pK_a values of some of the benzopyran-4-one derivatives that have been assayed as ARIs. In their study, the benzopyran derivative with a 7-hydroxyl group exhibited a pK_a value of 7.3, approaching the pH of the enzymatic assay and thus being partially in an anionic form. Conversely, the benzopyran derivative bearing a 7-methoxy substituent, in which proton dissociation was prevented, was found to be much less active. In our case, the electron-withdrawing F substituents confer a negative inductive effect, increasing the acidic character of the JF0064 hydroxyl groups. In fact, it has been reported that the pK_a value of 2,3,5,6-tetrafluorophenol is 5.53 (Kipper *et al.*, 2011). Note also that the short distance between the O atoms of the inner hydroxyl group of the inhibitor and Tyr48 (2.61 Å), in addition to the position of the H atom, which is clearly next to the tyrosine residue, indicates that this bond is likely to be a

short ionic hydrogen bond (Fuhrmann *et al.*, 2006), in agreement with the electrostatic character of the binding of JF0064 to the anionic site. In the corresponding AKR1B10 complex, the hydrogen-bond distances between Tyr49 OH and His111 $N^{\varepsilon 1}$ and the JF0064 hydroxyl group (2.64 and 2.59 Å, respectively) also agree with the proposed acidic character of the latter hydroxyl group. The lower resolution of the AKR1B10 complex (1.75 Å) does not allow the observation of any H atoms. However, as the inhibition pattern observed for JF0064 with both enzymes is equivalent, it is reasonable to expect that this hydroxyl group will also possess an acidic character in the latter case. Moreover, MD simulations with wild-type AKR1B10 holoenzyme complexed with JF0064 also support our observation. If Tyr50/49 is protonated (as has been observed for the AR–$NADP^+$–JF0064 complex), this analysis suggests that the inner hydroxyl group is deprotonated.

The second important point concerns the hydrogen bonds involving organic F atoms. This is a subject which has been discussed with some controversy (Dunitz, 2004); however, hydrogen bonds of the C—F···H—N or C—F···H—O types have been described previously for AR and AKR1C3 inhibitors (Lovering *et al.*, 2004; Rastelli *et al.*, 2002). In fact, the ultrahigh-resolution difference map shows a peak corresponding to the H atom of $N^{\varepsilon 1}$ of Trp111 directed towards F3 of JF0064 (Fig. 5), confirming the hydrogen bond to the F atom.

The MD simulations allowed us to obtain a model of the AKR1B10 holoenzyme complexed with JF0064. The superposition of this model with the AR cognate complex shows JF0064 to be nearly identically placed in both enzymes (Fig. 6*c*), with even the outer moiety (displaced towards loop B in the crystallized mAKR1B10 mutant; Fig. 3*a*) and the contacts with the outer hydroxyl group being similar. However, there is a difference which might account for the threefold difference in the IC_{50} values: the displacement of Phe122/Phe123. In AR, Phe122 is oriented towards the active site and seals the pocket more efficiently than Phe123 in AKR1B10, which points towards the solvent and exhibits a more open pocket (Fig. 6*d*). In fact, the MD suggested a subpocket next to loop A (including Phe123) which appears to be more loosely packed than in AR. The pocket accommodated a buried water molecule trapped inside it (data not shown), a process usually linked to an entropic penalty, as previously observed in the complex of AKR1B10 V301L with fidarestat (Ruiz *et al.*, 2013).

In summary, it can be concluded that for both AR and AKR1B10 the strong interaction with the anion-binding pocket accomplished by inhibitors with a carboxylic acid or a cyclic imide group (Bohren & Grimshaw, 2000) is matched by the binding of the acidic hydroxyl moiety of JF0064 in a non-competitive mode.

4.2. Perspectives of the JF0064 compound for drug design

JF0064 has emerged as a new lead compound targeting AR/AKR1B10. Previously, some compounds have been characterized as novel ARI/AKR1B10 inhibitors, and molecular-docking studies predicted hydrogen bonding to the anion-binding pocket *via* hydroxyl groups (Fig. 1*a* and Table 3). Similarly to JF0064, the inner hydroxyl group of these compounds is within hydrogen-bonding distance of the active-site catalytic Tyr or His residue. The distal hydroxyl (or carboxyl) group seems to interact with hydrophilic residues of loops A and C (except for AR and JF0064, in which the interaction is mediated by a network of ordered water molecules). Here, we show for the first time X-ray structures of AR/AKR1B10 complexed with an inhibitor exhibiting a substituted phenol moiety, which could be a good bioisosteric group for replacing the carboxylic acid (Ballatore *et al.*, 2013). The less acidic hydroxyl group should show improved pharmacokinetic and bioavailability profiles with respect to inhibitors with a carboxylic acid group.

The incorporation of halogen atoms into a lead drug candidate results in analogues that are usually more lipophilic; consequently, they are used to improve penetration through lipid membranes and tissues. Halogenation also enhances blood–brain barrier permeability and this is a prerequisite for drugs that need to target the central nervous system (Hernandes *et al.*, 2010; Parisini *et al.*, 2011). A first step for JF0064 drug optimization would be to assess whether the F atom is the best suited halogen or whether it could be replaced by a Cl or Br atom (which are of larger size and increasing hydrophobicity; Vallejos *et al.*, 2012). A second step would be to remove or to replace one or more halogen atoms in the phenol moieties, thus checking their importance in the interaction with the AR/AKR1B10 inhibitor-binding pocket. This removal/replacement would diminish the acidic character of the hydroxyl group in order to fine-tune the pharmacokinetic properties: on increasing the pK_a value from nearly 5.5 in JF0064 to 7, the compound would become uncharged in circulation (thus improving its ability to cross biological membranes) and charged once bound to the protein (the pK_a of the compound would decrease in this environment analogously to the case of cyclic imides; El-Kabbani & Podjarny, 2007).

It is known that any ligand-binding event displaces water molecules from a binding site. In structure-based drug design (SBDD), most of these water molecules are never explicitly considered because they are highly disordered and therefore rarely observed crystallographically. However, in this work, the ultrahigh resolution of the AR–JF0064 complex allows an estimation of whether these water molecules are displaceable by a given ligand moiety. Indeed, in the AR complex, two of the water molecules in the vicinity of the outer hydroxyl group, HOH-95 and HOH-71 (Fig. 4*a*), present very low *B* factors (∼11 $Å^2$). While these waters seem to be conserved in the AKR1B10 model obtained by MD, the surrounding amino acids in AR and AKR1B10 are different (Val297, Ala299 and Ser302 in AR *versus* Ala298, Asn300 and Gln303 in AKR1B10). This opens the possibility of modifying the inhibitor to occupy these positions with groups that make specific interactions, either with AR or with AKR1B10, to increase the selectivity and potency. In summary, analysis of the inhibition

properties of the JF compound series with AR and AKR1B10 has permitted the discovery of a novel lead compound, JF0064, which is able to inhibit both AR and AKR1B10. In this regard, some disease conditions overexpressing both proteins, such as hepatocellular carcinoma (Cao *et al.*, 1998; Zeindl-Eberhart *et al.*, 2004), could benefit from the use of a single compound to inhibit the two enzymes. This idea, to design a drug with pronounced target selectivity but covering one or more targets of interest, has lately gained credence (Huggins *et al.*, 2012). Furthermore, the screening performed here, complemented by structural data, has provided significant insights into the SBDD of potent and selective AR and AKR1B10 inhibitors.

We thank the IGBMC Structural Genomics Platform staff (in particular Pierre Poussin-Courmontagne and Dr Alastair McEwen). We also thank Dr Valérie Lamour and Dr Eduardo Howard for their helpful discussions about how to obtain AKR1B10 crystals. The crystallographic experiments were performed on the X06SA beamline at the Swiss Light Source synchrotron, Paul Scherrer Institut, Villigen, Switzerland. We thank in particular Takashi Tomizaki and Anuschka Pauluhn for their help in data collection. This work has been funded by the CNRS, the INSERM, the Université de Strasbourg, the Région Alsace, the Hôpital Civil de Strasbourg, Instruct (part of the European Strategy Forum of Research Infrastructures; ESFRI) and the French Infrastructure for Integrated Structural Biology (FRISBI) ANR-10-INSB-05-01, the Spanish Ministerio de Economía y Competitividad (BFU2011-24176), Generalitat de Catalunya (2009 SGR 795), the Fondation pour la Recherche Médicale (Code FRM: SPF20121226275) and the Bayer HealthCare 'Grants4Targets' program entitled 'AKR1B10 as a molecular target for cancer control' (2009–2010).

References

Adams, P. D. *et al.* (2010). *Acta Cryst.* D**66**, 213–221.

Ballatore, C., Huryn, D. M. & Smith, A. B. III (2013). *ChemMedChem*, **8**, 385–395.

Barski, O. A., Gabbay, K. H., Grimshaw, C. E. & Bohren, K. M. (1995). *Biochemistry*, **34**, 11264–11275.

Barski, O. A., Tipparaju, S. M. & Bhatnagar, A. (2008). *Drug Metab. Rev.* **40**, 553–624.

Biadene, M., Hazemann, I., Cousido, A., Ginell, S., Joachimiak, A., Sheldrick, G. M., Podjarny, A. & Schneider, T. R. (2007). *Acta Cryst.* D**63**, 665–672.

Bohren, K. M. & Grimshaw, C. E. (2000). *Biochemistry*, **39**, 9967–9974.

Calderone, V., Chevrier, B., Van Zandt, M., Lamour, V., Howard, E., Poterszman, A., Barth, P., Mitschler, A., Lu, J., Dvornik, D. M., Klebe, G., Kraemer, O., Moorman, A. R., Moras, D. & Podjarny, A. (2000). *Acta Cryst.* D**56**, 536–540.

Cao, D., Fan, S. T. & Chung, S. S. M. (1998). *J. Biol. Chem.* **273**, 11429–11435.

Case, D. A. *et al.* (2012). *Amber*12. University of California, San Francisco, USA. http://ambermd.org.

Changjin, Z. (2013). *Diabetes Mellitus – Insights and Perspectives*, edited by O. O. Oguntibeju, pp. 17–46. Rijeka: InTech.

Chung, Y. T., Matkowskyj, K. A., Li, H., Bai, H., Zhang, W., Tsao, M.-S., Liao, J. & Yang, G.-Y. (2012). *Mod. Pathol.* **25**, 758–766.

Costantino, L., Rastelli, G., Gamberini, M. C., Vinson, J. A., Bose, P., Iannone, A., Staffieri, M., Antolini, L., Del Corso, A., Mura, U. & Albasini, A. (1999). *J. Med. Chem.* **42**, 1881–1893.

Darden, T., York, D. & Pedersen, L. (1993). *J. Chem. Phys.* **98**, 10089.

Díez-Dacal, B., Gayarre, J., Gharbi, S., Timms, J. F., Coderch, C., Gago, F. & Pérez-Sala, D. (2011). *Cancer Res.* **71**, 4161–4171.

Dunitz, J. D. (2004). *Chembiochem*, **5**, 614–621.

El-Kabbani, O., Darmanin, C., Schneider, T. R., Hazemann, I., Ruiz, F., Oka, M., Joachimiak, A., Schulze-Briese, C., Tomizaki, T., Mitschler, A. & Podjarny, A. (2004). *Proteins*, **55**, 805–813.

El-Kabbani, O. & Podjarny, A. (2007). *Cell. Mol. Life Sci.* **64**, 1970–1978.

El-Kabbani, O., Ruiz, F., Darmanin, C. & Chung, R. P.-T. (2004). *Cell. Mol. Life Sci.* **61**, 750–762.

Emsley, P., Lohkamp, B., Scott, W. G. & Cowtan, K. (2010). *Acta Cryst.* D**66**, 486–501.

Endo, S., Matsunaga, T., Kuwata, K., Zhao, H.-T., El-Kabbani, O., Kitade, Y. & Hara, A. (2010). *Bioorg. Med. Chem.* **18**, 2485–2490.

Endo, S., Matsunaga, T., Mamiya, H., Ohta, C., Soda, M., Kitade, Y., Tajima, K., Zhao, H.-T., El-Kabbani, O. & Hara, A. (2009). *Arch. Biochem. Biophys.* **487**, 1–9.

Endo, S., Matsunaga, T., Soda, M., Tajima, K., Zhao, H.-T., El-Kabbani, O. & Hara, A. (2010). *Biol. Pharm. Bull.* **33**, 886–890.

Fenical, W., Jensen, P. R., Palladino, M. A., Lam, K. S., Lloyd, G. K. & Potts, B. C. (2009). *Bioorg. Med. Chem.* **17**, 2175–2180.

Fuente, J. A. de la & Manzanaro, S. (2003). *Nat. Prod. Rep.* **20**, 243–251.

Fuente, J. A. de la, Manzanaro, S., Martín, M. J., de Quesada, T. G., Reymundo, I., Luengo, S. M. & Gago, F. (2003). *J. Med. Chem.* **46**, 5208–5221.

Fuhrmann, C. N., Daugherty, M. D. & Agard, D. A. (2006). *J. Am. Chem. Soc.* **128**, 9086–9102.

Fukumoto, S. *et al.* (2005). *Clin. Cancer Res.* **11**, 1776–1785.

Gallego, O., Belyaeva, O. V., Porté, S., Ruiz, F. X., Stetsenko, A. V., Shabrova, E. V., Kostereva, N. V., Farrés, J., Parés, X. & Kedishvili, N. Y. (2006). *Biochem. J.* **399**, 101–109.

Gallego, O., Ruiz, F. X., Ardèvol, A., Domínguez, M., Alvarez, R., de Lera, A. R., Rovira, C., Farrés, J., Fita, I. & Parés, X. (2007). *Proc. Natl Acad. Sci. USA*, **104**, 20764–20769.

Götz, A. W., Williamson, M. J., Xu, D., Poole, D., Le Grand, S. & Walker, R. C. (2012). *J. Chem. Theory Comput.* **8**, 1542–1555.

Gregson, R. M., Glidewell, C., Ferguson, G. & Lough, A. J. (2000). *Acta Cryst.* B**56**, 39–57.

Harrison, D. H., Bohren, K. M., Ringe, D., Petsko, G. A. & Gabbay, K. H. (1994). *Biochemistry*, **33**, 2011–2020.

Hernandes, M. Z., Cavalcanti, S. M. T., Moreira, D. R. M., de Azevedo, W. F. Jr & Leite, A. C. L. (2010). *Curr. Drug Targets*, **11**, 303–314.

Hornak, V., Abel, R., Okur, A., Strockbine, B., Roitberg, A. & Simmerling, C. (2006). *Proteins*, **65**, 712–725.

Howard, E. I., Sanishvili, R., Cachau, R. E., Mitschler, A., Chevrier, B., Barth, P., Lamour, V., Van Zandt, M., Sibley, E., Bon, C., Moras, D., Schneider, T. R., Joachimiak, A. & Podjarny, A. (2004). *Proteins*, **55**, 792–804.

Huggins, D. J., Sherman, W. & Tidor, B. (2012). *J. Med. Chem.* **55**, 1424–1444.

Humphrey, W., Dalke, A. & Schulten, K. (1996). *J. Mol. Graph.* **14**, 33–38.

Jakalian, A., Bush, B. L., Jack, D. B. & Bayly, C. I. (2000). *J. Comput. Chem.* **21**, 132–146.

Jakalian, A., Jack, D. B. & Bayly, C. I. (2002). *J. Comput. Chem.* **23**, 1623–1641.

Jarman, M., Barrie, S. E., Deadman, J. J., Houghton, J., McCague, R. & Rowlands, M. G. (1990). *J. Med. Chem.* **33**, 2452–2455.

Jorgensen, W. L., Chandrasekhar, J., Madura, J. D., Impey, R. W. & Klein, M. L. (1983). *J. Chem. Phys.* **79**, 926.

Kim, Y. *et al.* (2008). *Nature Methods*, **5**, 853–854.

Kipper, K., Herodes, K. & Leito, I. (2011). *J. Chromatogr. A*, **1218**, 8175–8180.
Lamour, V., Barth, P., Rogniaux, H., Poterszman, A., Howard, E., Mitschler, A., Van Dorsselaer, A., Podjarny, A. & Moras, D. (1999). *Acta Cryst.* D**55**, 721–723.
Lecomte, C., Jelsch, C., Guillot, B., Fournier, B. & Lagoutte, A. (2008). *J. Synchrotron Rad.* **15**, 202–203.
Le Grand, S., Götz, A. W. & Walker, R. C. (2013). *Comput. Phys. Commun.* **184**, 374–380.
Liu, Z., Zhong, L., Krishack, P. A., Robbins, S., Cao, J. X., Zhao, Y., Chung, S. & Cao, D. (2009). *Gene*, **437**, 39–44.
Loncharich, R. J., Brooks, B. R. & Pastor, R. W. (1992). *Biopolymers*, **32**, 523–535.
Lovering, A. L., Ride, J. P., Bunce, C. M., Desmond, J. C., Cummings, S. M. & White, S. A. (2004). *Cancer Res.* **64**, 1802–1810.
Ma, J., Yan, R., Zu, X., Cheng, J.-M., Rao, K., Liao, D.-F. & Cao, D. (2008). *J. Biol. Chem.* **283**, 3418–3423.
Manzanaro, S., Salva, J. & de la Fuente, J. A. (2006). *J. Nat. Prod.* **69**, 1485–1487.
Martin, R. (2000). *Handbook of Hydroxybenzophenones*, p. 423. Dordrecht: Kluwer Academic Publishers.
Matsunaga, T., Endo, S., Soda, M., Zhao, H.-T., El-Kabbani, O., Tajima, K. & Hara, A. (2009). *Biochem. Biophys. Res. Commun.* **389**, 128–132.
Murshudov, G. N., Skubák, P., Lebedev, A. A., Pannu, N. S., Steiner, R. A., Nicholls, R. A., Winn, M. D., Long, F. & Vagin, A. A. (2011). *Acta Cryst.* D**67**, 355–367.
Navaza, J. (2001). *Acta Cryst.* D**57**, 1367–1372.
Oates, P. J. (2008). *Curr. Drug Targets*, **9**, 14–36.
O'Boyle, N. M., Banck, M., James, C. A., Morley, C., Vandermeersch, T. & Hutchison, G. R. (2011). *J. Cheminform.* **3**, 33.
Otwinowski, Z. & Minor, W. (1997). *Methods Enzymol.* **276**, 307–326.
Parisini, E., Metrangolo, P., Pilati, T., Resnati, G. & Terraneo, G. (2011). *Chem. Soc. Rev.* **40**, 2267–2278.
Penning, T. M. (2005). *Clin. Cancer Res.* **11**, 1687–1690.
Podjarny, A., Cachau, R. E., Schneider, T., Van Zandt, M. & Joachimiak, A. (2004). *Cell. Mol. Life Sci.* **61**, 763–773.
Prince, E., Finger, L. W. & Konnert, J. H. (2006). *International Tables for Crystallography*, Vol. *C*, edited by E. Prince, pp. 694–701. Dordrecht: Kluwer Academic Publishers.
Quinn, A. M., Harvey, R. G. & Penning, T. M. (2008). *Chem. Res. Toxicol.* **21**, 2207–2215.
Ramana, K. V. & Srivastava, S. K. (2010). *Int. J. Biochem. Cell Biol.* **42**, 17–20.
Ramunno, A., Cosconati, S., Sartini, S., Maglio, V., Angiuoli, S., La Pietra, V., Di Maro, S., Giustiniano, M., La Motta, C., Da Settimo, F., Marinelli, L. & Novellino, E. (2012). *Eur. J. Med. Chem.* **51**, 216–226.
Rastelli, G., Antolini, L., Benvenuti, S. & Costantino, L. (2000). *Bioorg. Med. Chem.* **8**, 1151–1158.
Rastelli, G., Costantino, L., Gamberini, M. C., Del Corso, A., Mura, U., Petrash, J. M., Ferrari, A. M. & Pacchioni, S. (2002). *Bioorg. Med. Chem.* **10**, 1427–1436.
Rayment, I. (1997). *Methods Enzymol.* **276**, 171–179.
Rayment, I., Rypniewski, W. R., Schmidt-Bäse, K., Smith, R., Tomchick, D. R., Benning, M. M., Winkelmann, D. A., Wesenberg, G. & Holden, H. M. (1993). *Science*, **261**, 50–58.
Roe, D. R. & Cheatham, T. E. (2013). *J. Chem. Theory Comput.* **9**, 3084–3095.
Ruiz, F. X., Cousido-Siah, A., Mitschler, A., Farrés, J., Parés, X. & Podjarny, A. (2013). *Chem. Biol. Interact.* **202**, 178–185.
Ruiz, F. X., Gallego, O., Ardèvol, A., Moro, A., Domínguez, M., Alvarez, S., Alvarez, R., de Lera, A. R., Rovira, C., Fita, I., Parés, X. & Farrés, J. (2009). *Chem. Biol. Interact.* **178**, 171–177.
Ruiz, F. X., Porté, S., Parés, X. & Farrés, J. (2012). *Front. Pharmacol.* **3**, 58.
Ryckaert, J.-P., Ciccotti, G. & Berendsen, H. J. C. (1977). *J. Comput. Phys.* **23**, 327–341.
Salomon-Ferrer, R., Götz, A. W., Poole, D., Le Grand, S. & Walker, R. C. (2013). *J. Chem. Theory Comput.* **9**, 3878–3888.
Sheldrick, G. M. (2008). *Acta Cryst.* A**64**, 112–122.
Shinde, P. B., Lee, Y. M., Dang, H. T., Hong, J., Lee, C.-O. & Jung, J. H. (2008). *Bioorg. Med. Chem. Lett.* **18**, 6414–6418.
Sledz, P., Zheng, H., Murzyn, K., Chruszcz, M., Zimmerman, M. D., Chordia, M. D., Joachimiak, A. & Minor, W. (2010). *Protein Sci.* **19**, 1395–1404.
Soda, M., Endo, S., Matsunaga, T., Zhao, H.-T., El-Kabbani, O., Iinuma, M., Yamamura, K. & Hara, A. (2012). *Biol. Pharm. Bull.* **35**, 2075–2080.
Soda, M., Hu, D., Endo, S., Takemura, M., Li, J., Wada, R., Ifuku, S., Zhao, H.-T., El-Kabbani, O., Ohta, S., Yamamura, K., Toyooka, N., Hara, A. & Matsunaga, T. (2012). *Eur. J. Med. Chem.* **48**, 321–329.
Steuber, H., Heine, A., Podjarny, A. & Klebe, G. (2008). *J. Mol. Biol.* **379**, 991–1016.
Takemura, M., Endo, S., Matsunaga, T., Soda, M., Zhao, H.-T., El-Kabbani, O., Tajima, K., Iinuma, M. & Hara, A. (2011). *J. Nat. Prod.* **74**, 1201–1206.
Tammali, R., Reddy, A. B., Saxena, A., Rychahou, P. G., Evers, B. M., Qiu, S., Awasthi, S., Ramana, K. V. & Srivastava, S. K. (2011). *Carcinogenesis*, **32**, 1259–1267.
Tang, W. H., Martin, K. A. & Hwa, J. (2012). *Front. Pharmacol.* **3**, 87.
Urzhumtsev, A., Tête-Favier, F., Mitschler, A., Barbanton, J., Barth, P., Urzhumtseva, L., Biellmann, J. F., Podjarny, A. & Moras, D. (1997). *Structure*, **5**, 601–612.
Vallejos, M. J., Auffinger, P. & Ho, P. S. (2012). *International Tables for Crystallography*, Vol. *F*, edited by E. Arnold, D. M. Himmel & M. G. Rossmann, pp. 821–826. Chichester: John Wiley & Sons.
Verma, M., Martin, H. J., Haq, W., O'Connor, T. R., Maser, E. & Balendiran, G. K. (2008). *Eur. J. Pharmacol.* **584**, 213–221.
Walter, T. S., Meier, C., Assenberg, R., Au, K. F., Ren, J., Verma, A., Nettleship, J. E., Owens, R. J., Stuart, D. I. & Grimes, J. M. (2006). *Structure*, **14**, 1617–1622.
Wang, C., Yan, R., Luo, D., Watabe, K., Liao, D.-F. & Cao, D. (2009). *J. Biol. Chem.* **284**, 26742–26748.
Wang, J., Wolf, R. M., Caldwell, J. W., Kollman, P. A. & Case, D. A. (2004). *J. Comput. Chem.* **25**, 1157–1174.
Wang, R., Wang, G., Ricard, M. J., Ferris, B., Strulovici-Barel, Y., Salit, J., Hackett, N. R., Gudas, L. J. & Crystal, R. G. (2010). *Chest*, **138**, 1402–1410.
Yadav, U. C., Mishra, R., Aguilera-Aguirre, L., Sur, S., Bolodgh, I., Ramana, K. V. & Srivatsava, S. K. (2013). *Inflamm. Allergy Drug Targets*, **12**, 178–186.
Zeindl-Eberhart, E., Haraida, S., Liebmann, S., Jungblut, P. R., Lamer, S., Mayer, D., Jäger, G., Chung, S. & Rabes, H. M. (2004). *Hepatology*, **39**, 540–549.
Zhang, L., Zhang, H., Zhao, Y., Li, Z., Chen, S., Zhai, J., Chen, Y., Xie, W., Wang, Z., Li, Q., Zheng, X. & Hu, X. (2013). *FEBS Lett.* **587**, 3681–3686
Zhao, H.-T., Soda, M., Endo, S., Hara, A. & El-Kabbani, O. (2010). *Eur. J. Med. Chem.* **45**, 4354–4357.